crystals

MDPI

Article

Completing the Ba–As Compositional Space: Synthesis and Characterization of Three New Binary Zintl Arsenides, Ba_3As_4, Ba_5As_4, and $Ba_{16}As_{11}$

Spencer R. Watts [1], Lindsey M. Wingate [1], Svilen Bobev [2] and Sviatoslav Baranets [1,*]

[1] Department of Chemistry, Louisiana State University, Baton Rouge, LA 70803, USA; swatt15@lsu.edu (S.R.W.); lwinga1@lsu.edu (L.M.W.)
[2] Department of Chemistry and Biochemistry, University of Delaware, Newark, DE 19716, USA; bobev@udel.edu
* Correspondence: sbaranets@lsu.edu

Abstract: Three novel binary barium arsenides, Ba_3As_4, Ba_5As_4, and $Ba_{16}As_{11}$, were synthesized and their crystal and electronic structures were investigated. Structural data collected via the single-crystal X-ray diffraction method indicate that the anionic substructures of all three novel compounds are composed of structural motifs based on the homoatomic As–As contacts, with $[As_2]^{4-}$ dimers found in Ba_5As_4 and $Ba_{16}As_{11}$, and an $[As_4]^{6-}$ tetramer found in Ba_3As_4. Ba_3As_4 and Ba_5As_4 crystallize in the orthorhombic crystal system—with the non-centrosymmetric space group *Fdd2* (a = 15.3680(20) Å, b = 18.7550(30) Å, c = 6.2816(10) Å) for the former, and the centrosymmetric space group *Cmce* (a = 16.8820(30) Å, b = 8.5391(16) Å, and c = 8.6127(16) Å) for the latter—adopting Eu_3As_4 and Eu_5As_4 structure types, respectively. The heavily disordered $Ba_{16}As_{11}$ structure was solved in the tetragonal crystal system with the space group $P\bar{4}2_1m$ (a = 12.8944(12) Å and c = 11.8141(17) Å). The Zintl concept can be applied to each of these materials as follows: $Ba_3As_4 = (Ba^{2+})_3[As_4]^{6-}$, $Ba_5As_4 = (Ba^{2+})_5(As^{3-})_2[As_2]^{4-}$, and $2 \times Ba_{16}As_{11} = (Ba^{2+})_{32}(As^{3-}) \approx {}_{20}[As_2]^{4-} \approx 1$, pointing to the charge-balanced nature of these compounds. Electronic structure calculations indicate narrow bandgap semiconducting behavior, with calculated bandgaps of 0.47 eV for Ba_3As_4, 0.34 eV for Ba_5As_4, and 0.33 eV for $Ba_{16}As_{11}$.

Keywords: Zintl phases; semiconductors; single-crystal X-ray diffraction; crystal structures; structural disorder

Citation: Watts, S.R.; Wingate, L.M.; Bobev, S.; Baranets, S. Completing the Ba–As Compositional Space: Synthesis and Characterization of Three New Binary Zintl Arsenides, Ba_3As_4, Ba_5As_4, and $Ba_{16}As_{11}$. *Crystals* **2024**, *14*, 570. https://doi.org/10.3390/cryst14060570

Academic Editor: Andrei Vladimirovich Shevelkov

Received: 22 May 2024
Revised: 11 June 2024
Accepted: 17 June 2024
Published: 20 June 2024

1. Introduction

Exploration into Zintl phases has been a growing field of interest in recent years, as they have shown to exhibit unique structural motifs and great potential for various applications [1,2]. Zintl phases are defined as a subclass of intermetallic materials in which structures, both ionic and covalent bonding can coexist. This is because an electropositive metal (typically from group 1, 2, or the lanthanide block), when combined with an electronegative element from groups 13 to 15, can be considered as an electron donor that becomes a cation. The electrons are accepted by the other atoms in the structure, which become anions and/or use the electrons to form bonds and to satisfy their octets. In this parlance, the interactions between the cations and the anionic sublattice are viewed as electrostatic, while the rest of the chemical bonding is regarded as covalent. Thus, a charge balance in Zintl phases is an inherent feature that can be readily explained and predicted by the basic valence principles.

A large subclass of Zintl compounds contain pnictogens, i.e., elements from group 15 (*Pn* = P, As, Sb, Bi), and can be referred to as Zintl pnictides. By combining pnictogens with different alkali, alkaline earth, or rare earth metals, numerous Zintl pnictides with a wide array of structural motifs have been discovered and characterized [3]. The electron transfer

between constituting elements of different electronegativity often yields Zintl materials with narrow bandgaps and excellent electronic and transport properties, thus making them suitable candidates for thermoelectric applications [2,4,5].

The ability of pnictogen atoms to form homoatomic bonds noticeably diversifies the structural abundance of Zintl pnictides [3]. Examples of such can be seen in many different materials, with $[P_{plane}]^{1-}$ square layers present in $LnSiP_3$ (Ln = La, Ce) [6], P^- helices in Ba_3P_5Cl [7], and zigzag $[Pn_4]^{4-}$ tetramers in A_5Pn_4 (A = K, Rb, Cs and Pn = As, Sb, Bi) [8], as well as materials with multiple anionic subunit types, such as $A_{11}Pn_{10}$ (A = Ca, Sr, Ba, Eu, Yb and Pn = P, As, Sb, Bi) with linear $[Pn_2]^{4-}$ dumbbells and square $[Pn_4]^{4-}$ units, $Ca_2As_3 = Ca_8As_{12}$ with $[As_4]^{6-}$ and $[As_8]^{8-}$ oligomers, or $A_{14}MPn_{11}$ (A = Ca, Sr, Ba, Eu; M = Al, Mn, Zn, Cd; Pn = P, As, Sb, Bi) with linear $[Pn_3]^{7-}$ trimer and $[MPn_4]$ tetrahedra [9–11]. These structural motifs exemplify the diversity of the observed covalent substructures within Zintl pnictides and their great potential for studying structure-property relationships.

Recent efforts on Zintl pnictide exploration have been primarily focused on developing novel ternary or multinary compounds [2,12], yet compositionally simpler binary phases are still occasionally discovered [13–18]. Our initial experiments were focused on the development of novel thermoelectric oxyarsenides [19], which, despite being known for decades, remain relatively underexplored, with multiple predicted but yet-to-be-discovered compounds [20]. Additionally, recent reports indicate their great promise for thermoelectric applications [21]. While developing this project, we identified several unreported compounds within the Ba–As phase diagram. This system is somewhat underexplored compared to other compositionally similar alkaline earth metal pnictide families, primarily due to the pronounced air sensitivity of barium arsenides and the toxicity of arsenic and its compounds. In this paper, we report the synthesis and structural analysis of three novel binary Zintl arsenides: Ba_3As_4, Ba_5As_4, and $Ba_{16}As_{11}$. We also provide insights into their electronic structures and bonding, highlighting their charge-balanced nature and semiconducting behavior.

2. Materials and Methods

2.1. Synthesis

All starting materials [barium rods (Thermo Scientific, Waltham, MA, USA, 99%) and arsenic granules (Thermo Scientific, 99.999%)] and reaction products were stored and handled inside an argon-filled glovebox ($p(O_2) \leq 1$ ppm). Barium was filed before use to remove oxidated coatings. Ba_3As_4 and Ba_5As_4 were originally discovered during metal flux reactions targeting quaternary oxypnictide phases. However, these samples were multiphase, so direct reactions were attempted. Single crystals of Ba_3As_4, Ba_5As_4, and $Ba_{16}As_{11}$ were obtained via stoichiometric combinations of Ba:As (totaling about 500 mg of product per reaction), which were then placed in 3/8″ OD niobium tubes and arc-welded shut under argon. These tubes were then sealed in evacuated fused silica ampoules. The temperature profile for the synthesis of Ba_5As_4 and $Ba_{16}As_{11}$ was as follows: (1) heat to 1100 °C at a rate of 100 °C/h, (2) hold at 1100 °C for 20 h, (3) then cool at a rate of 5 °C/h to 100 °C, followed by the removal of reactions from the furnace. The temperature profile for the synthesis of Ba_3As_4 involved lower reaction temperatures, with (1) heating to 800 °C at a rate of 200 °C/h, (2) holding at 800 °C for 20 h, (3) then cooling to room temperature at a rate of 5 °C/h. Ampoules were opened in the glovebox following cooling, and crystals were removed and studied via diffraction methods.

All three phases are air- and moisture-sensitive, which prevented comprehensive studies of physical properties, although we could synthesize sizable single crystals of Ba_3As_4 and Ba_5As_4 by employing flux methods.

> *CAUTION! Arsenic and arsenic-containing compounds are highly hazardous. Proper personal protective equipment should be utilized when handling arsenic-containing compounds. Arsenic sublimes at 614 °C, which is significantly below the synthetic temperatures for these materials. As arsane gas can form from the slow hydrolysis of*

arsenide-bearing compounds, reactions must be performed in contained, well-ventilated areas, and crucibles and lab equipment may not be cleaned with water prior to slow oxidation. Arsenic may react with niobium at high temperatures with the formation of unadvertised side products.

2.2. Structural Characterization

Data for Ba_3As_4 and Ba_5As_4 were all collected at 100 K using a Bruker APEX II diffractometer (Bruker, Billerica, MA, USA) equipped with Mo Kα radiation (λ = 0.71073 Å), whereas $Ba_{16}As_{11}$ data were collected with a Bruker D8 Venture Duo diffractometer using Ag radiation (λ = 0.56086 Å). Suitably sized single crystals were selected under the microscope and mounted on MiTeGen plastic loops attached to the goniometer head. Data integration and absorption correction were performed with the SAINT and SADABS program packages (version 2.03) [22,23]. Crystal structures were solved by utilizing the SHELXT program, with structure refinement performed using full-matrix least squares methods on F^2 with SHELXL, using Olex2 software (version 1.5) as a graphical interface [24–27]. The STRUCTURE TIDY program was used to standardize coordinates [28]. Selected details of the data collection and crystallographic parameters, such as atomic coordinates and bond distances, are provided in Tables 1, 2 and S1.

Table 1. Selected data collection details and crystallographic data for Ba_3As_4, Ba_5As_4, and $Ba_{16}As_{11}$ (T = 100(2) K).

	Ba_3As_4	**Ba_5As_4**	**$Ba_{16}As_{11.07(2)}$** [b]
Space Group	*Fdd2*	*Cmce*	$P\bar{4}2_1m$
Structure Type	Eu_3As_4	Eu_5As_4	$Ca_{16}Sb_{11}$
fw/g mol^{-1}	711.70	986.38	3027.18
a/Å	15.3680(20) Å	16.8820(30) Å	12.8944(12) Å
b/Å	18.7550(30) Å	8.5391(16) Å	a
c/Å	6.2816(10) Å	8.6127(16) Å	11.8141(17) Å
V/Å^3	1810.526 Å^3	1241.582 Å^3	1964.278 Å^3
Z	8	4	2
ρ_{calc}/g cm^{-3}	5.22	5.28	5.12
μ/mm^{-1}	27.32 (MoKα)	26.14 (MoKα)	13.11 (AgKα)
Collected/Independent Reflections	5225/1035	5566/815	38,038/3160
R_1 ($I > 2\sigma_{(I)}$) [a]	0.0257	0.0482	0.0380
wR_2 ($I > 2\sigma_{(I)}$) [a]	0.0409	0.0663	0.0737
R_1 (all data) [a]	0.0313	0.0688	0.0410
wR_2 (all data) [a]	0.0423	0.0703	0.0749
$\Delta\rho_{max,min}$/e$^-$ Å^{-3}	1.27/−2.01	2.08/−2.15	2.00/−2.22
CCDC Deposition Number	2353584	2353585	2353586

[a] $R_1 = \Sigma\,||F_o|-|F_c||/\Sigma|F_o|$. $wR_2 = (\Sigma\,[w(F_o^2 - F_c^2)^2]/\Sigma wF_o^4)^{1/2}$, $w = 1/[\sigma^2(F_o^2) + (AP)^2 + (BP)]$, where $P = (F_o^2 + 2F_c^2)/3$; A and B are weight coefficients. [b] $Ba_{16}As_{11}$ notation is used throughout the manuscript.

Table 2. Select As–As bond lengths from Ba_3As_4, Ba_5As_4, and $Ba_{16}As_{11}$.

Structure	Bond	Bond Length
Ba_3As_4	As1–As1 As1–As2	2.548 Å 2.468 Å
Ba_5As_4	As1–As1	2.551 Å
$Ba_{16}As_{11}$	As1A–As1A As6A–As6A	2.462 Å 2.597 Å

2.3. Electronic Structure Calculations

Experimentally observed unit cell parameters and atomic coordinates of ordered Ba_3As_4 and Ba_5As_4 compounds were used for calculations. Two unique barium positions and two unique arsenic positions were used for each experimental model (Tables S1 and S2). For $Ba_{16}As_{11}$, a disorder-free model with fully occupied non-split sites was developed for calculations with six unique barium positions and six unique arsenic positions (Table S3). Details of the electronic structure, including Total and Projected density of states (DOS) and band structure, were investigated with the TB-LMTO-ASA Program after the convergence of the total energy on the dense k-mesh, with $10 \times 10 \times 10$ points for Ba_3As_4 and Ba_5As_4 and $10 \times 10 \times 11$ points for $Ba_{16}As_{11}$ in the Brillouin zone [29]. Empty spheres were introduced to satisfy atomic sphere approximation (ASA) and the von Barth–Hedin exchange correlation functional was utilized [30]. The Fermi level was selected as the energy reference ($E_F = 0$ eV). A basic set included Ba [6s, 4d, 6p](4f) and As [4s, 4p](4d), with the downfolded orbitals presented in parentheses. Chemical bonding analysis was performed by calculating the energy contributions of all filled electronic states for selected atom pairs via the Crystal Orbital Hamilton Population (COHP) method [31]. It should be noted that for the calculations within the TB-LMTO-ASA framework, unoptimized cells were used, which leads to some uncertainty for the bandgap size estimation. These limitations leave room for more advanced characterizations and simulations.

3. Results and Discussion

3.1. Synthesis

The initial discovery of the title compounds occurred during the attempted synthesis of multinary barium oxyarsenide materials—work that is still ongoing, and the results of which will be presented in a future article. While our first reactions produced novel ternary barium oxyarsenides, the title binary barium arsenides were found to be the main products. All three presented compounds were identified as black single crystals sensitive to air and moisture, that rapidly decayed when removed from the inert gas-protected environment. Such instability significantly complicated powder XRD characterization and made routine physical properties studies practically impossible. The synthetic conditions listed in the experimental section are favorable in producing noticeable amounts of the title materials, although some single crystals of Ba_3As_4 can be obtained in the reactions with the intended introduction of oxygen. Notably, Ba_3As_4 has been previously reported [32], although its crystal structure is not found in structural databases.

Ba_5As_4 was found to be a major product of its intended reaction, though its phase purity could not be reasonably determined due to the air sensitivity. The Ba_3As_4 sample contained Ba_3As_4 as a major product, with some Ba_5As_4 present as well. Synthetic attempts to produce Ba_3As_4 using stoichiometric ratios of reactants at higher temperatures only yielded Ba_5As_4, leading us to believe that the "5–4" phase is more thermodynamically favorable at higher temperatures. Exploration into the $Ba_{16}As_{11}$ phase originally began due to its exclusion from an original extensive survey into the $A_{16}Pn_{11}$ phases (A = Ca, Sr, Ba; Pn = As, Sb) reported by Corbett more than two decades ago [33]. While the authors failed to produce the $Ba_{16}As_{11}$ phase, their suggested optimized synthetic procedures involving direct reactions in sealed metal tubes proved successful for making $Ba_{16}As_{11}$ in bulk by using an elevated temperature profile of 1100 °C, as compared to prior attempts

involving annealing at 850–900 °C. This previous report also indicates the need for synthesis under a dynamic vacuum to eliminate hydrogen impurities in the metals; however, this does not appear to be an issue in our reactions. This falls in line with the results of the recently reported $Ba_{16}Sb_{11}$ [15]. The synthesis of $Ba_{16}As_{11}$ always produces a mixed product of $Ba_{16}As_{11}$ and Ba_4As_3 (or rather, As-deficient $Ba_4As_{2.67}$) [34]. This mixture is reasonably expected, due to the nearly identical Ba:As ratio for both compounds (Figure 1). The single crystal diffraction and electronic structure study of Ba_4As_3 has been reported previously [34–37], but the existence of $Ba_{16}As_{11}$ has never been predicted.

Compositional space within the Ba–As binary system is heavily populated with multiple reported compositions in experimental (ICSD) and theoretical (OQMD) databases: $BaAs_2$, $BaAs_3$, $Ba_4As_{2.6}$, Ba_3As_{14}, Ba_5As_4, Ba_3As_2, BaAs, Ba_5As_3, and Ba_3As_4 [34,35,38–42] (Figure 1). Note that the title Ba_3As_4 and Ba_5As_4 were only theoretically predicted, being accessible from OQMD, but the structural elucidation of both will be presented in this work.

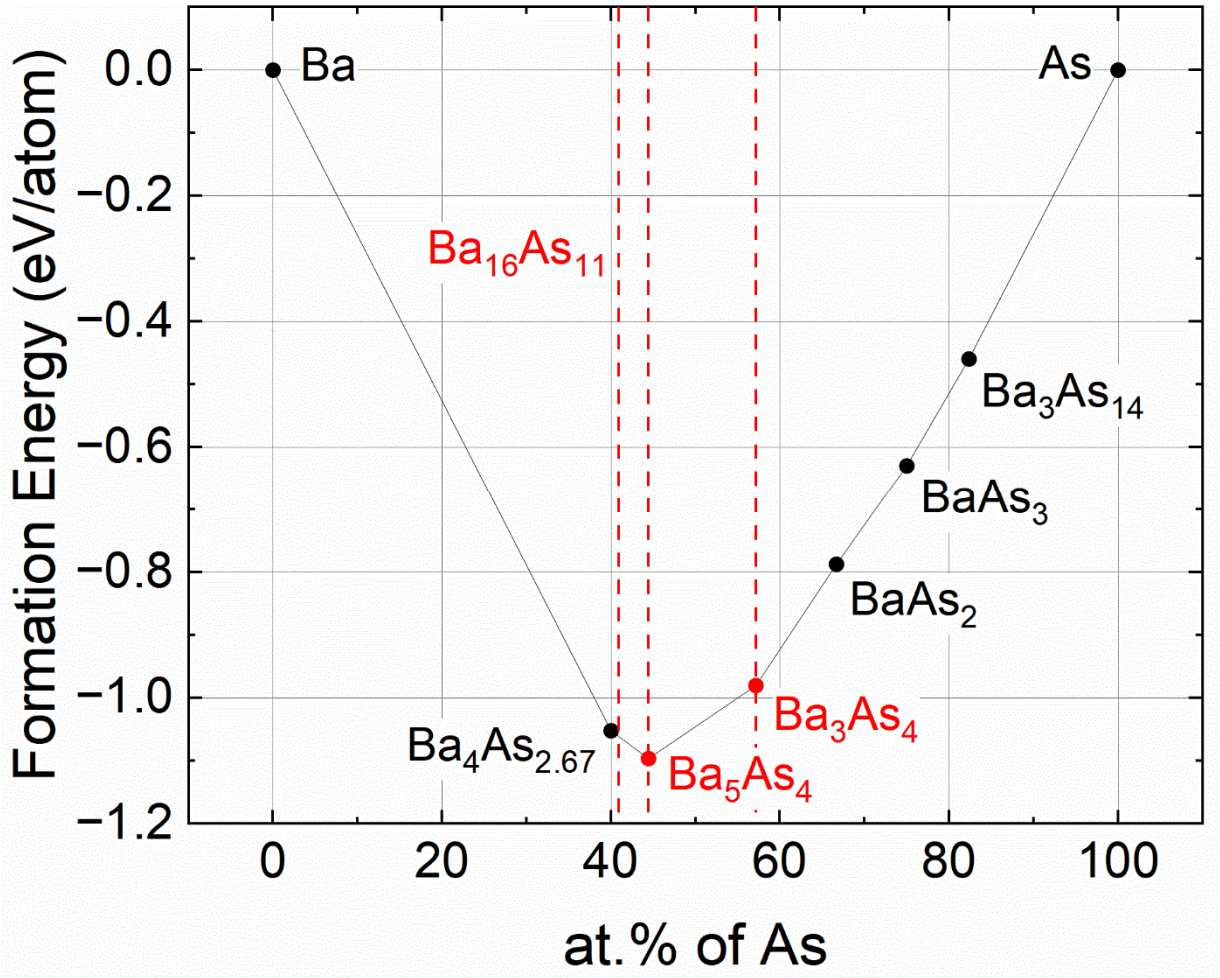

Figure 1. Phase diagram with reported formation energies of selected barium arsenides [35–37,41,42]. New phases reported in this paper are highlighted in red. The formation energy for $Ba_{16}As_{11}$ is not provided as it was not reported/predicted.

We did not attempt to further explore periodic trends, as most of the isostructural pnictides were already reported. These materials do prove to follow known periodic trends, such as those of as phosphides (Ba_3P_4 [43], Ba_5P_4 [13,44]), arsenides (Sr_3As_4 [45], Eu_5As_4 [46], Eu_3As_4 [47]), and antimonides (Ba_5Sb_4 [48,49], $Ba_{16}Sb_{11}$ [15]), to name a few; although, we do not exclude the possibility that the occasional discovery of some missing binary compounds within the structure types presented here is highly probable.

3.2. Crystal Structure and Bonding

The archetypes for all three reported compounds are well known and, therefore, do not require an extensive description of their crystal structures. In the following paragraphs, we will provide only a brief description focusing on the most important structural features.

3.2.1. Crystal Structure of Ba_3As_4

Our structural description will begin with Ba_3As_4. This compositionally and structurally simple compound crystallizes in the non-centrosymmetric orthorhombic space group *Fdd*2 and belongs to the Sr_3As_4 structure type [45], which is known to host multiple A_3Pn_4 phosphides and arsenides (A = Eu, Sr, Ba; Pn = P, As) [45,47,50]. Ba_3As_4 was initially discovered by von Schnering [43] and, while this work was underway, was structurally evaluated in the dissertation of Hermann [32], but the structural entry was not (and is still not) available in the ICSD (access date 21 March 2024) [51]. Our results corroborate well with the reported studies, although we observed slightly larger unit cell volumes despite lower data collection temperatures (Table 1).

According to the structural representation shown in Figure 2, one Ba_3As_4 formula unit consists of three Ba^{2+} cations and an oligomer of four As atoms joined via homoatomic covalent bonds, thus formulated as $[As_4]^{6-}$. There are two crystallographically independent Ba sites and two As sites occupying the 16b general position, with the exception of the special Ba2 8*a* site, yielding the Wyckoff sequence b^3a and the Pearson code *oF*56. The structure is made up of 1/3 empty $[Ba_6]$ and 2/3 arsenic-centered $[AsBa_6]$ triangular prisms, sharing their rectangular faces in either parallel or perpendicular fashion to the three-fold axis of the prism (Figure 2).

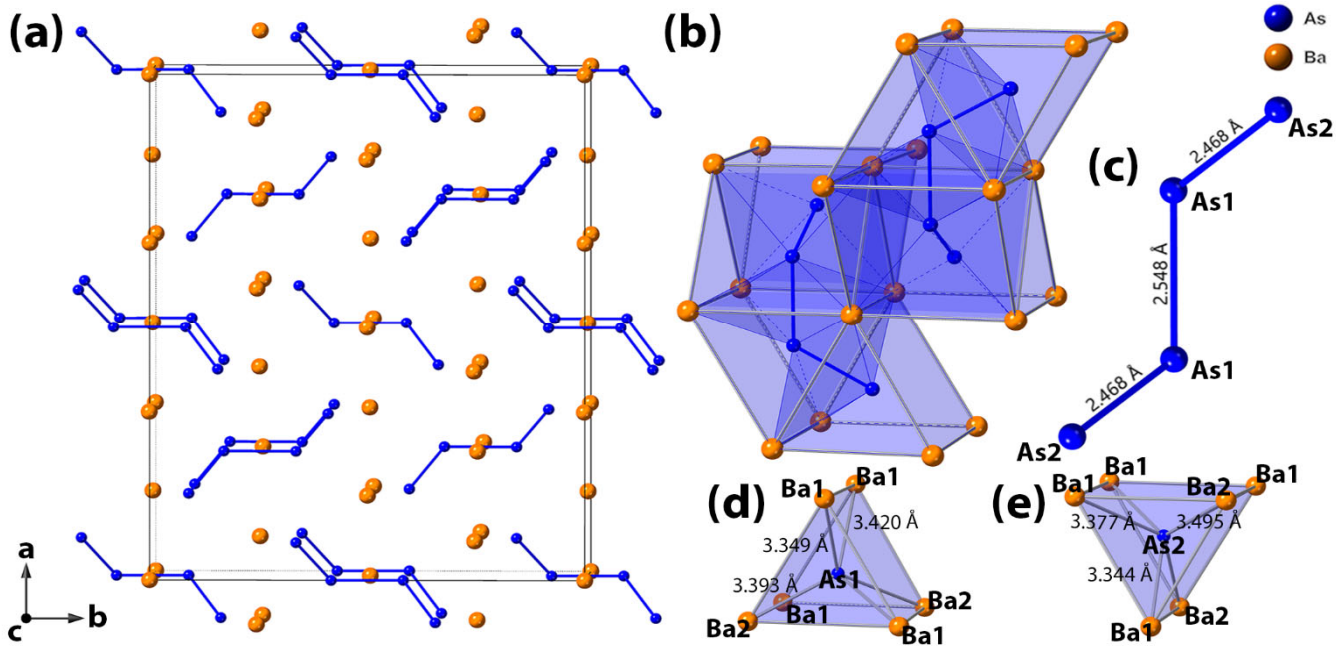

Figure 2. (**a**) The Ba_3As_4 structure, with highlighted $[As_4]^{6-}$ tetramers, and the outlined unit cell; (**b**) the trigonal prismatic arrangement of As-centred $[AsBa_6]$ polyhedra; (**c**) a close-up view of the $[As_4]^{6-}$ Zintl anion, with reported interatomic As−As distances; (**d**,**e**) a distinct representation of the As-centered coordination polyhedra for As1 and As2. Barium atoms are shown in orange and arsenic atoms are shown in blue.

Each $[As_4]^{6-}$ complex anion is nested within two pairs of mutually perpendicular $[AsBa_6]$ prisms, breaking the fragment into two symmetric [As1–As2] units. The arsenic atoms in this symmetric oligomer are linked in the [As2–As1–As1–As2] fashion. This four-membered fragment is located on a 2-fold rotation axis perpendicular to the *ab* plane,

and intersects the center of the As1–As1 bond. The refined As1–As2 and As1–As1 distances are ca. 2.47 Å and 2.55 Å, respectively. Both numbers are comparable with the doubled covalent radius of As [52], as well as with the reported As–As distances in Eu_3As_4, Sr_3As_4, and several other ternary Zintl arsenides [45,53]. Ba–As distances are in the range of 3.27–3.50 Å, being close to the sum of the covalent radii of Ba and As and to the values observed for known Zintl barium arsenides [34,38–40].

3.2.2. Crystal Structure of Ba_5As_4

Ba_5As_4, being more structurally complex, belongs to the Eu_5As_4 structure type [46], crystallizing in the orthorhombic space group *Cmce*. This family of Zintl pnictides is less explored, with only three reported compositions: Eu_5As_4, Ba_5P_4, and Ba_5Sb_4 [13,46,48]. Akin to Ba_3As_4, barium-rich Ba_5As_4 also consists of two Ba (16*g* and 4*a*) and two As (8*d* and 8*f*) sites, yielding the Wyckoff sequence *gfda* and the Pearson code *o*C36. We could synthesize only one modification of Ba_5As_4, although the compositionally related Ba_5P_4 phase is known to be dimorphic [13,44].

Ba_3As_4 and Ba_5As_4 structures are noticeably different. Half of the arsenic atoms in the latter dimerize, forming a homoatomic $[As_2]^{4-}$ dumbbell with an As1–As1 distance of ca. 2.55 Å (Figure 3). This is slightly longer than the doubled covalent radius of arsenic (2.38 Å) and in the compositionally similar Zintl arsenides, such as K_5As_4 (2.45 Å) [8,52], but is comparable to the reported As–As bond length for isostructural analogs, such as Eu_5As_4 (2.54 Å) [46].

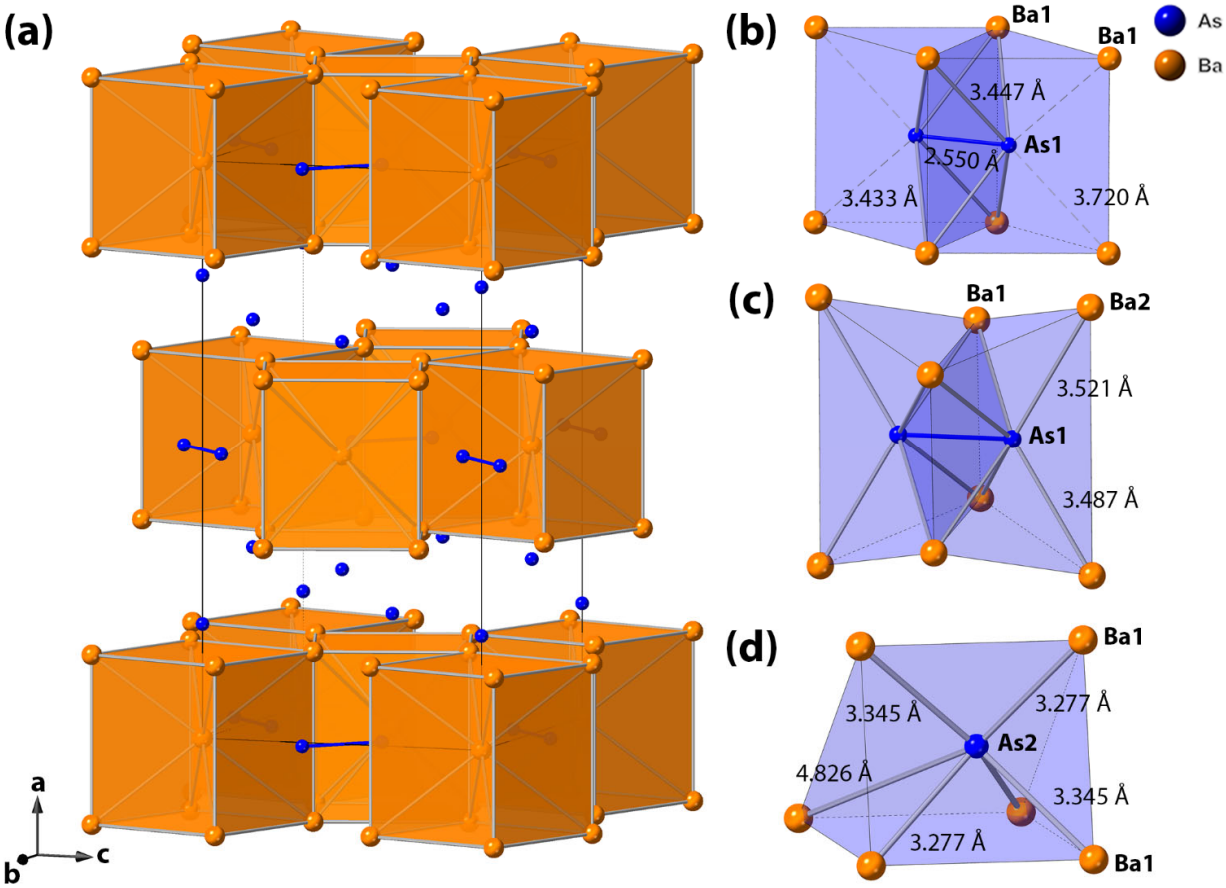

Figure 3. (**a**) A representation of the Ba_5As_4 structure, with slabs made of [$BaBa_8$] cubes, and the outlined unit cell. As–As dimers are located between the cubes; (**b**,**c**) the trigonal prismatic arrangements of As-centered [$AsBa_6$] polyhedra encasing the $[As_2]^{4-}$ anions; (**d**) a representation of As2-centered distorted trigonal prisms of Ba atoms. The color code is the same as in Figure 1.

Each As1 atom composing the dumbbell is 6-coordinated by four Ba1 and two Ba2 atoms in a distorted trigonal prismatic fashion (Figure 3c). Alternatively, [As_2] dimer can be viewed as enclosed between four adjacent [Ba2@$Ba1_8$] cubes that form the slab perpendicular to the *a*-axis (Figure 3a). In such an arrangement, the [As_2] unit is located within a pair of edge-sharing trigonal prisms with slightly off-centered As atoms, evidenced by slightly elongated Ba–As contacts (Figure 3b, Table S5). This slab of face-sharing [$AsBa_6$] and [$BaBa_8$] cubes alternates with another slab of As-centered distorted [Ba_6] trigonal prisms centered by As2 atoms (Figure 3d). With all prisms centered by As atoms and cubes centered by Ba atoms, the structure can be viewed as an intergrowth of Mo_2FeB_2- and FeB-types [54,55].

3.2.3. Crystal Structure of $Ba_{16}As_{11}$

$Ba_{16}As_{11}$ is the most complex structure of the three compounds discussed in this paper (Figure 4). It crystallizes in the tetragonal space group $P\bar{4}2_1m$ and shares a structure with the $Ca_{16}Sb_{11}$ archetype [33], despite being much more heavily disordered. This puts the structure more in line with our recent report on the $Ba_{16}Sb_{11}$ phase, where we comprehensively discussed crystal structure, polymorphism, and details of the disorder within this family of compounds [15].

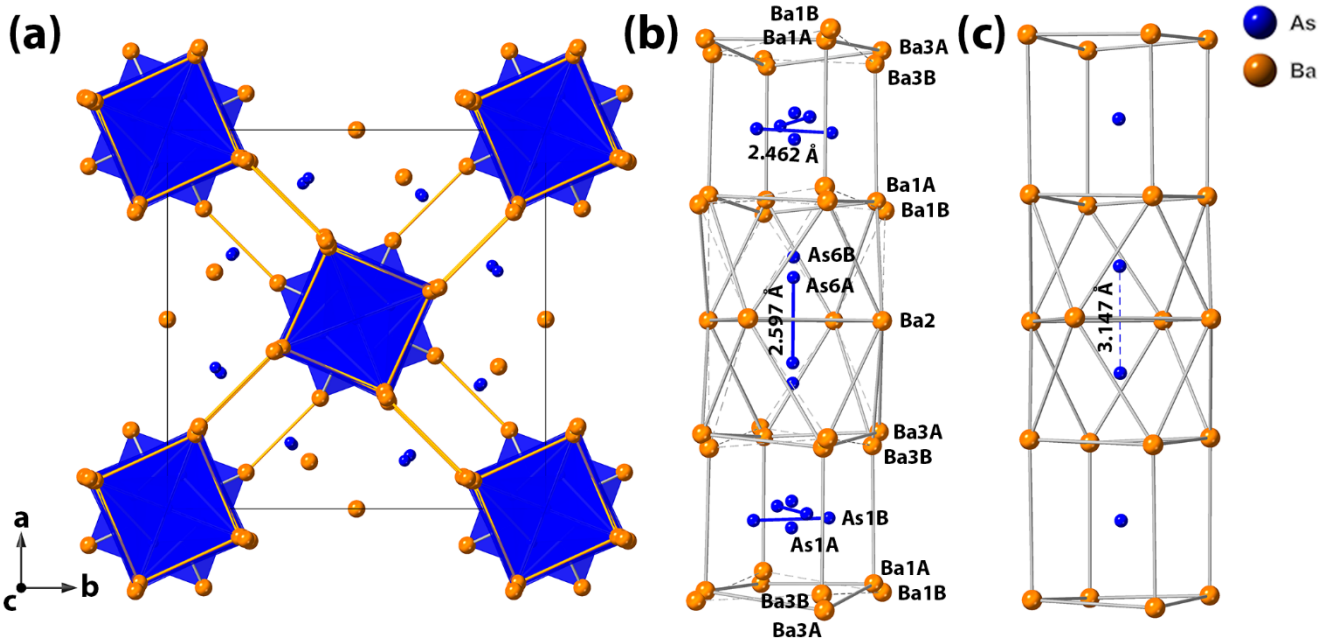

Figure 4. (**a**) A view of the $Ba_{16}As_{11}$ structure along the [001] direction, with outlined barium polyhedra. The unit cell is highlighted; (**b**) the characteristic square prism–antiprism column, with all details of the structural disorder; (**c**) the simplified structural model used for electronic structure calculations. Note the noticeably elongated As6–As6 contact. The color code is the same as in Figure 1.

The $A_{16}Pn_{11}$ (A = Ca, Sr, Ba, Eu, Yb; Pn = P, As, Sb, Bi) family of compounds comprises more than a dozen reported compositions [15,33,56], although the title $Ba_{16}As_{11}$ phase is reported in this paper for the first time. Unlike the $Ba_{16}Sb_{11}$ phase, which crystallizes in a disordered tetragonal structure of the $Ca_{16}Sb_{11}$-type and an ordered monoclinic coloring variant of the $La_{16}Rh_8Sn_3$-type [57], we identified only the disordered tetragonal version of the $Ba_{16}As_{11}$ phase, which could be partially due to the thermodynamic stability of the compositionally similar Ba_4As_3 phase (Figure 1). We do not exclude the possibility that the ordered monoclinic phase exists and could be discovered in the future.

The collected single-crystal X-ray diffraction data can readily produce a structure solution in space group $P\bar{4}2_1m$, although from the subsequent refinements, we observed a severe disorder nearly identical to that in the recently reported $Ba_{16}Sb_{11}$ structure [15].

In the following paragraphs, we will briefly introduce details of the crystal structure and some differences between the title compounds and previously reported structural analogs.

Similarly to the $Ba_{16}Sb_{11}$ phase, the hallmark of the crystal structure of $Ba_{16}As_{11}$ is best described as an arrangement of columns composed of [Ba_8] distorted square prisms and antiprisms that host disordered As1 and As6 atoms (Figure 4a). Each site is split into two positions, with As1A/As1B residing within the prisms and As6A/As6B occupying the antiprisms (Figure 4b). The disorder of the As1 site, although less pronounced compared to that of Sb1 in $Ba_{16}Sb_{11}$, still reveals a non-negligible occupancy of the As1B site (Wyckoff 8*f*), with a site occupancy factor (SOF) of 0.034(4). Combined with the SOF of 0.468(7) for the As1A site (Wyckoff 4*d*), we yield the slightly off-stoichiometric composition of $Ba_{16}As_{11.07(2)}$, similar to the situation in the isostructural $Ba_{16}Sb_{11.2(1)}$ [15]. For simplification, we use the simplified $Ba_{16}As_{11}$ formula throughout the manuscript, although the reader should be aware that the refined composition is non-stoichiometric for both barium arsenide and antimonide. The higher multiplicity of the As1B site allows for the presence of any of two pairs of As1B–As1B homoatomic bonds that are ca. 2.46 Å long. The presence of these partially occupied atomic sites is required to achieve the charge balance, as can be evidenced below.

Additional modeling was required in order to resolve the observed anomalous displacement parameter of As6, formally located in the center of the adjacent antiprism (Figure 4b). The split of the As6 site into two As6A and As6B sites (Wyckoff 4*d*), with SOFs of 0.543(3) and 0.466(3), respectively, is necessitated for achieving electronic stabilization through the formation of homoatomic, although slightly elongated, As6A–As6A contacts of ca. 2.60 Å (Table S3). Given the partial occupancy of the As6A site, the observed [As_2] dimer cannot account for a full bond per unit cell.

The described disorder of several As sites results in the concomitant positional disorder of the surrounding Ba sites, and goes even further through a domino effect that causes the disorder of As5 sites and concomitant Ba sites. However, the shared face of the antiprisms that host As6 atoms is made up of non-disordered Ba2 atoms, which has previously been observed for several binary pnictides [15,33,58]. The $[As6Ba_8]_{antiprism}$-$[As6Ba_8]_{antiprism}$-$[As1Ba_8]_{prism}$ columns are oriented along the *c*-axis and they are linked through the relatively short Ba2–Ba2, Ba1–Ba1, and Ba3–Ba3 contacts in the range of 3.58–3.90 Å. While these values are smaller than the sum of the covalent radii of Ba, they represent an interaction between two cations, thus exceeding the doubled sum of ionic radii [59]. In addition, the partial occupancy of multiple Ba sites corroborates well with the observation of such comparatively short distances [15,38–40].

3.2.4. Structural Relationships and Charge Balance Considerations

Despite adopting different structures, the Ba_3As_4, Ba_5As_4, and $Ba_{16}As_{11}$ phases share similar structural features and polyanionic arrangements. We discussed the bonding largely in the context of the framework of trigonal/square prisms/antiprisms and cubes composed of Ba and centered by As atoms. Ba–As bond distances within these polyhedra adopt a wide range of values, including 3.27–3.50 Å for Ba_3As_4, 3.28–3.52 Å for Ba_5As_4, and 3.20–3.64 Å for $Ba_{16}As_{11}$. These values are close to the sum of the covalent radii of Ba and As, and to the values observed for known binary and ternary Zintl arsenides [34,38–40,60].

As the structural complexity increases from the relatively simple Ba_3As_4 and Ba_5As_4 compounds to the heavily disordered $Ba_{16}As_{11}$ compound, arsenic atoms become more reduced, due to the decreased number of homoatomic As–As contacts per formula unit. All As atoms in the Ba_3As_4 phase are linked to the $[As_4]^{6-}$ tetramer, with terminal and central As atoms being formally charged at −2 and −1, respectively. Such fully ionic approximation results in the charge-balanced composition of $(Ba^{2+})_3[As_4]^{6-}$, where Ba atoms are considered electron donors in accordance with the Zintl concept [1]. A quite similar bonding situation is observed for the Ba_5As_4 phase, where only one half of the arsenic atoms in the structure are dimerized, yielding the charge-balanced $(Ba^{2+})_5[As_2]^{4-}(As^{3-})_2$ composition, considering the fully ionic approximation.

A significant increase in disorder for the $Ba_{16}As_{11}$ structure results in a less straightforward Zintl count, which is in line with the previously reported $Ba_{16}Sb_{11}$ phase [15]. The presence of the homoatomic As1B–As1B and As6A–As6A bonds allows for careful rationalization of the structure and composition with the Zintl count, expressed as $(Ba^{2+})_{16}(As^{3-})_{9.87}([As_2]^{4-})_{0.60}(h^+)_{0.01}$ (with h^+ representing an electron-hole). Apparently, the presence of extensive disorder, as well as a deviation from the ideal "16–11" composition, is required for achieving the charge-balanced composition.

3.3. Electronic Structure

Barium and arsenic have a moderate electronegativity difference (with Pauling electronegativities of 0.89 and 2.18, respectively) [61], which supports the expectation of a sizable charge transfer and, therefore, semiconducting behavior. The latter suggestion is supported by the Zintl concept rationalization of the charge balance, discussed in the previous section. The results of the electronic structure calculations, presented in Figures 5–7, corroborate well with the predicted charge-balanced nature of the title compounds and provide further insights into chemical bonding within these compounds.

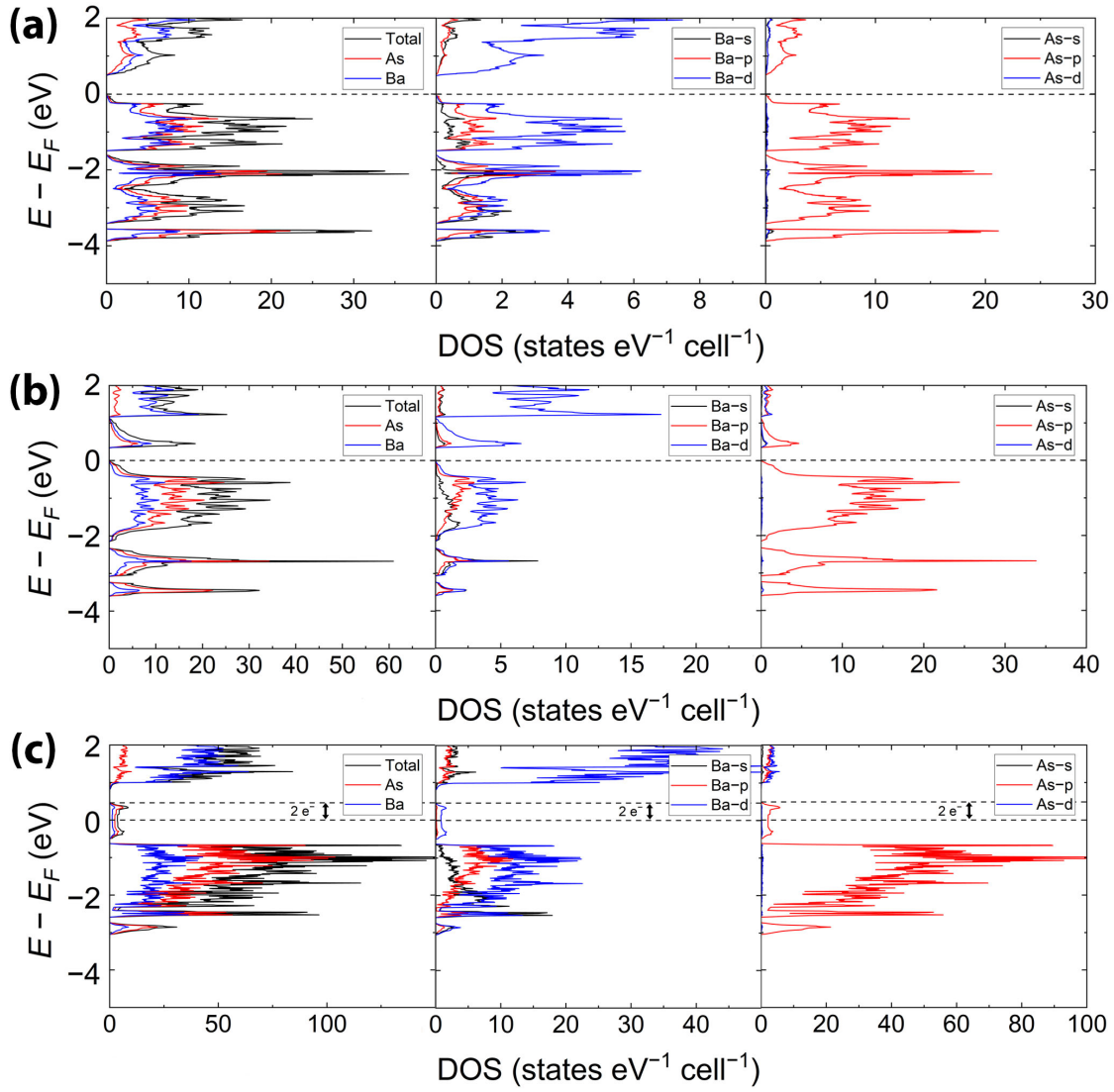

Figure 5. Calculated Total (DOS) and Partial (PDOS) density of states plots for (**a**) Ba_3As_4, (**b**) Ba_5As_4, and (**c**) $Ba_{16}As_{11}$. The Fermi level is the energy reference at 0 eV. An additional dashed line for (**c**) at ca. 0.48 eV indicates a 2-electron shift per unit cell, which corresponds to 1 electron per formula unit.

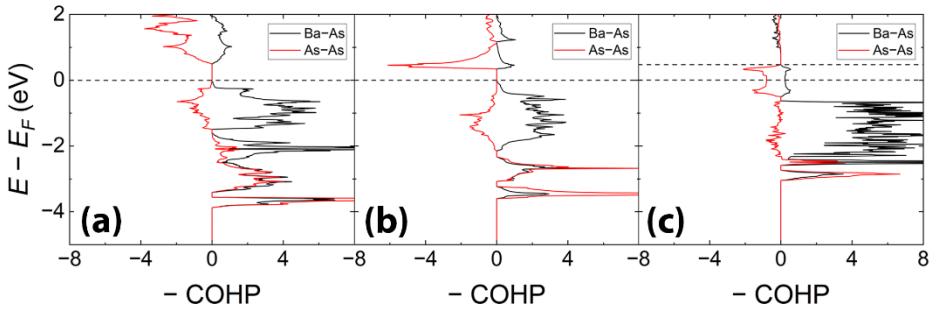

Figure 6. Calculated Crystal Orbital Hamilton plots (COHP) for (**a**) Ba_3As_4, (**b**) Ba_5As_4, and (**c**) $Ba_{16}As_{11}$. The Fermi level is the energy reference at 0 eV. An additional dashed line at ca. 0.48 eV indicates a 1-electron shift per formula unit.

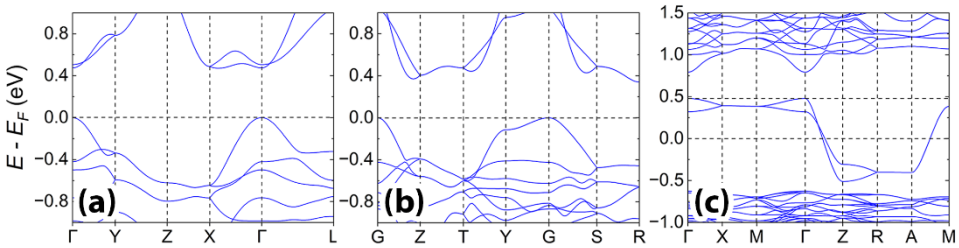

Figure 7. Band structures for (**a**) Ba_3As_4, (**b**) Ba_5As_4, and (**c**) $Ba_{16}As_{11}$. The Fermi level is the energy reference at 0 eV. An additional dashed line at ca. 0.48 eV indicates a 1-electron shift per formula unit.

As we mentioned in the Materials and Methods section, the disorder-free natures of Ba_3As_4 and Ba_5As_4 allowed us to study their electronic structures using the experimentally obtained cell parameters and atomic coordinates. Both compounds can be classified as narrow gap semiconductors, with a calculated direct bandgap opening of ca. 0.47 eV for Ba_3As_4 and an indirect bandgap of 0.34 eV for Ba_5As_4, making them small bandgap semiconductors. The Total and Partial density of states (DOS) plots show similar patterns to other Zintl pnictides. States within the valence band in the area of −12 eV to −8 eV consist primarily of As-s states, while states above −4 eV to the valence band maxima (VBM) consist of As-p states (Figure 5), indicating poor hybridization of the As orbitals. Ba-s, Ba-p, and Ba-d states all contribute towards the same range, with Ba-d being the dominant orbital contribution. The multiple observed interactions between Ba and As within the discussed polyhedra, as well as the large coordination numbers of the Ba atoms in these compounds, support the idea that Ba-d orbitals are essential for the formation of multiple Ba–As bonds.

The study of the electronic structure of $Ba_{16}As_{11}$ is complicated by the severe disorder of multiple Ba and As sites (Figure 4b). However, we generated a simplified structural model composed of fully occupied atomic sites, which preserves the reported bonding pattern (Figure 4c), although the As6–As6 contacts of 3.15 Å are noticeably elongated. The As1 site in the simplified model is located at the origin, occupying the 2*a* Wyckoff site. The lower multiplicity of As1 in the simplified model, compared to the As1A and As1B sites in the refined structure (Table S3), is compensated by the SOF of 1, thus yielding the $Ba_{16}As_{11}$ stoichiometric composition, which is nearly identical to the refined one. However, the lack of As–As bonding results in an unbalanced composition, which can be described as $(Ba^{2+})_{16}(As^{3-})_{11}(h^+)$, considering a fully ionic approximation. It becomes evident that the top of the valence band should be shifted upwards to ca. 0.48 eV, to align with a direct bandgap opening of 0.31 eV (Figure 5c). This 0.48 eV difference corresponds to 1 electron per formula unit, indicating that the charge balance can only be achieved with the presence of the As–As pair. Besides a Fermi level shift, the Total and Partial DOS plots for $Ba_{16}As_{11}$ share similar features to those discussed for the Ba_3As_4 and Ba_5As_4 phases.

Nearly identical observations can be made for the electronic structure of the Ba_4As_3 phase. This phase was found to be a minor product of $Ba_{16}As_{11}$ synthesis, and its formation can be anticipated given their similar compositions (Figure 1). Our structural data on this compound corroborates well with the earlier structural reports [34], where the observation of the partial SOF for As was justified to fulfill the charge balance according to the notation $(Ba^{2+})_4(As^{3-})_{2.67}$. Our calculations on the disorder-free $(Ba^{2+})_2(As^{3-})_3(h^+)$ composition also indicate the necessity of the Fermi level shift (Figure S1), similarly to the $Ba_{16}As_{11}$ case discussed above.

Plotting the COHP curves for each compound allowed us to examine the bonding situation further. The COHP analysis indicates that the Ba–As bonds in all reported compounds are optimized. The average integrated COHP (−ICOHP) values for the Ba–As bonds in each species were found to be as follows: 0.81 eV/bond for Ba_3As_4, 0.44 eV/bond for Ba_5As_4, and 0.75 eV/bond for $Ba_{16}As_{11}$, indicating significant charge transfer, as can be anticipated for bonds made of two elements with a large difference in electronegativity. Conversely, the calculated −ICOHP values for the As–As bonds in Ba_3As_4 and Ba_5As_4 are noticeably larger, adopting values of −2.51 eV/bond and 2.62 eV/bond, respectively. These noticeably larger values point to stronger covalency of these homoatomic contacts compared to the Ba–As bonds. On the other hand, the −ICOHP values for the As6–As6 long contacts in $Ba_{16}As_{11}$ are close to 0, indicating nearly non-bonding states.

4. Conclusions

The discovery and structural characterization of three novel binary Zintl arsenides—Ba_3As_4, Ba_5As_4, and $Ba_{16}As_{11.07}$—significantly enriches the Ba–As phase diagram, increasing the number of known barium arsenides by more than 50%. All compounds can be characterized within the Zintl–Klemm formalism, featuring homoatomic covalently bonded As–As contacts that accept electrons from electropositive Ba cations. They are predicted to be charge-balanced narrow-gap semiconductors through the charge partitioning $Ba_3As_4 = (Ba^{2+})_3[As_4]^{6-}$, $Ba_5As_4 = (Ba^{2+})_5(As^{3-})_2[As_2]^{4-}$, and $Ba_{16}As_{11.07} = (Ba^{2+})_{16}(As^{3-})_{9.87}([As_2]^{4-})_{0.60}$, and electronic structure calculations. Ba_3As_4 and Ba_5As_4 are structurally ordered stoichiometric compounds, whereas $Ba_{16}As_{11.07}$ is heavily disordered, with the positional disorder responsible for the formation of partially occupied As–As contacts and, therefore, achieving the charge balance. The electronic structure of the compositionally similar $Ba_4As_{2.67}$ phase was also studied, although the charge balance in the latter is achieved through the occupational disorder.

By expanding the exploration of these binary A_xPn_y systems (A = Ca, Sr, Ba, Eu; Pn = P, As, Sb, Bi) through comprehensive studies of crystal and electronic structures, as well as the tunability of transport properties, we can establish a comprehensive understanding of the structure-property relationships necessary to understand the perspective of binary Zintl pnictides for a greater range of potential applications.

Supplementary Materials: The following supporting information can be downloaded at: https://www.mdpi.com/article/10.3390/cryst14060570/s1, Table S1: Refined atomic coordinates for Ba_3As_4, Table S2: Refined atomic coordinates for Ba_5As_4, Table S3: Refined atomic coordinates for $Ba_{16}As_{11}$, Table S4: Bond distances for Ba_3As_4, Table S5: Bond distances for Ba_5As_4, Table S6: Select bond distances for $Ba_{16}As_{11}$, Figure S1: Details of the electronic structure of Ba_4As_3.

Author Contributions: Investigation, S.R.W.; validation, L.M.W.; formal analysis, S.R.W. and S.B. (Sviatoslav Baranets); data curation, S.R.W. and L.M.W.; writing—original draft preparation, S.R.W.; visualization, S.R.W.; writing—review and editing, S.B. (Sviatoslav Baranets) and S.B. (Svilen Bobev); methodology, conceptualization, supervision, project administration, funding acquisition, S.B. (Sviatoslav Baranets). All authors have read and agreed to the published version of the manuscript.

Funding: This research project was financially sponsored by the College of Science and the Department of Chemistry at Louisiana State University (start-up funding). Sviatoslav Baranets also acknowledges the Louisiana State Board of Regents, under Award LEQSF (2024-27)-RD-A-06. S.

Bobev acknowledges financial support from the United States Department of Energy, Office of Science, Basic Energy Sciences, under Award #DE-SC0008885.

Data Availability Statement: The corresponding crystallographic information files (CIF) have been deposited into the Cambridge Crystallographic Database Centre (CCDC) and can be obtained, free of charge, via https://www.ccdc.cam.ac.uk/structures/ (accessed on 20 May 2024) or by emailing data_request@ccdc.cam.ac.uk with the following depository numbers: 2353584-2353586.

Conflicts of Interest: The authors declare no conflicts of interest.

References

1. Nesper, R. The Zintl-Klemm concept—A historical survey. *Z. Anorg. Allg. Chem.* **2014**, *640*, 2639–2648. [CrossRef]
2. Kauzlarich, S.M. Zintl Phases: From Curiosities to Impactful Materials. *Chem. Mater.* **2023**, *35*, 7355–7362. [CrossRef] [PubMed]
3. Baranets, S.; Ovchinnikov, A.; Bobev, S. Structural diversity of the Zintl pnictides with rare-earth metals. In *Handbook on the Physics and Chemistry of Rare Earths*; Elsevier: Amsterdam, The Netherlands, 2021; Volume 60, pp. 227–324.
4. Islam, M.M.; Kauzlarich, S.M. The Potential of Arsenic-based Zintl Phases as Thermoelectric Materials: Structure & Thermoelectric Properties. *Z. Anorg. Allg. Chem.* **2023**, *649*, e202300149.
5. Liu, K.-F.; Xia, S.-Q. Recent progresses on thermoelectric Zintl phases: Structures, materials and optimization. *J. Solid State Chem.* **2019**, *270*, 252–264. [CrossRef]
6. Akopov, G.; Mark, J.; Viswanathan, G.; Lee, S.J.; McBride, B.C.; Won, J.; Perras, F.A.; Paterson, A.L.; Yuan, B.; Sen, S. Third time's the charm: Intricate non-centrosymmetric polymorphism in $LnSiP_3$ (Ln = La and Ce) induced by distortions of phosphorus square layers. *Dalton Trans.* **2021**, *50*, 6463–6476. [CrossRef] [PubMed]
7. Ishtiyak, M.; Samarakoon, S.G.K.; Don, T.K.; Watts, S.R.; Baranets, S. Novel ternary Zintl phosphide halides Ba_3P_5X (X = Cl, Br) with 1D helical phosphorus chains: Synthesis, crystal and electronic structure. *Nanoscale* **2024**, *16*, 7916–7925. [CrossRef] [PubMed]
8. Gascoin, F.; Sevov, S.C. Synthesis and Characterization of the "Metallic Salts" A_5Pn_4 (A = K, Rb, Cs and Pn = As, Sb, Bi) with Isolated Zigzag Tetramers of Pn_4^{4-} and an Extra Delocalized Electron. *Inorg. Chem.* **2001**, *40*, 5177–5181. [CrossRef]
9. Rehr, A.; Kauzlarich, S.M. $Sr_{11}Sb_{10}$. *Acta Crystallogr. Sect. C Cryst. Struct. Commun.* **1994**, *50*, 1859–1861. [CrossRef]
10. Liang, Y.; Cardoso-Gil, R.; Schnelle, W.; Zhao, J.-T.; Grin, Y. Synthesis, crystal structure and physical properties of $Yb_{11}Bi_{10-x}Sn_x$. *Solid State Sci.* **2013**, *18*, 127–130. [CrossRef]
11. Hu, Y.; Cerretti, G.; Wille, E.L.K.; Bux, S.K.; Kauzlarich, S.M. The remarkable crystal chemistry of the $Ca_{14}AlSb_{11}$ structure type, magnetic and thermoelectric properties. *J. Solid State Chem.* **2019**, *271*, 88–102. [CrossRef]
12. Ovchinnikov, A.; Bobev, S. Zintl phases with group 15 elements and the transition metals: A brief overview of pnictides with diverse and complex structures. *J. Solid State Chem.* **2019**, *270*, 346–359. [CrossRef]
13. Dolyniuk, J.-A.; He, H.; Ivanov, A.S.; Boldyrev, A.I.; Bobev, S.; Kovnir, K. Ba and Sr binary phosphides: Synthesis, crystal structures, and bonding analysis. *Inorg. Chem.* **2015**, *54*, 8608–8616. [CrossRef] [PubMed]
14. Hoffmann, A.V.; Hlukhyy, V.; Fässler, T.F. Crystal structure of undecacalcium decaarsenide, $Ca_{11}As_{10}$. *Z. Für Krist. New Cryst. Struct.* **2023**, *238*, 1–3. [CrossRef]
15. Baranets, S.; Ovchinnikov, A.; Samarakoon, S.G.K.; Bobev, S. Synthesis, crystal and electronic structure of the Zintl phase $Ba_{16}Sb_{11}$. A case study uncovering greater structural complexity via monoclinic distortion of the tetragonal $Ca_{16}Sb_{11}$ structure type. *Z. Anorg. Und Allg. Chem.* **2023**, *649*, e202300148. [CrossRef]
16. Samarakoon, S.G.K.; Ovchinnikov, A.; Baranets, S.; Bobev, S. Ba_5Sb_8: The Highest Homologue of the Family of Binary Semiconducting Barium Antimonides Ba_nSb2_{n-2} ($n \geq 2$). *Inorganics* **2023**, *12*, 3. [CrossRef]
17. Dobrokhotova, Z.V.; Zaitsev, A.; Zemchenko, M.; Litvina, A.; Mogutnov, B.; Yaschenko, S. Thermodynamic properties of calcium and barium phosphides. *J. Therm. Anal.* **1992**, *38*, 1113–1122. [CrossRef]
18. Hoffmann, A.V.; Hlukhyy, V.; Fässler, T.F. Ca_4As_3—A new binary calcium arsenide. *Acta Crystallogr. Sect. E Crystallogr. Commun.* **2015**, *71*, 1548–1550. [CrossRef]
19. Baranets, S.; Darone, G.M.; Bobev, S. Structural diversity among multinary pnictide oxides: A minireview focused on semiconducting and superconducting heteroanionic materials. *Z. Für Krist. Cryst. Mater.* **2022**, *237*, 1–26. [CrossRef]
20. Shen, J.; Hegde, V.I.; He, J.; Xia, Y.; Wolverton, C. High-throughput computational discovery of ternary mixed-anion oxypnictides. *Chem. Mater.* **2021**, *33*, 9486–9500. [CrossRef]
21. Rahim, W.; Skelton, J.M.; Scanlon, D.O. Ca_4Sb_2O and Ca_4Bi_2O: Two promising mixed-anion thermoelectrics. *J. Mater. Chem. A* **2021**, *9*, 20417–20435. [CrossRef]
22. *SAINT*; BrukerAXS Inc.: Fitchburg, WI, USA, 2014.
23. *SADABS*; BrukerAXS Inc.: Fitchburg, WI, USA, 2014.
24. Sheldrick, G.M. Crystal structure refinement with SHELXL. *Acta Crystallogr. Sect. C Struct. Chem.* **2015**, *71*, 3–8. [CrossRef] [PubMed]
25. Sheldrick, G.M. SHELXT—Integrated space-group and crystal-structure determination. *Acta Crystallogr. Sect. A Found. Adv.* **2015**, *71*, 3–8. [CrossRef] [PubMed]

26. Dolomanov, O.V.; Bourhis, L.J.; Gildea, R.J.; Howard, J.A.; Puschmann, H. OLEX2: A complete structure solution, refinement and analysis program. *J. Appl. Crystallogr.* **2009**, *42*, 339–341. [CrossRef]
27. Sheldrick, G.M. *XPREP*; Bruker AXS Inc.: Madison, WI, USA, 2018.
28. Gelato, L.; Parthé, E. STRUCTURE TIDY—A computer program to standardize crystal structure data. *J. Appl. Crystallogr.* **1987**, *20*, 139–143. [CrossRef]
29. Krier, G.; Jepsen, O.; Burkhardt, A.; Andersen, O. *The TB-LMTO-ASA Program*; Max-Planck-Institut für Festkörperforschung: Stuttgart, Germany, 1995.
30. Von Barth, U.; Hedin, L. A local exchange-correlation potential for the spin polarized case. i. *J. Phys. C Solid State Phys.* **1972**, *5*, 1629. [CrossRef]
31. Dronskowski, R.; Bloechl, P.E. Crystal orbital Hamilton populations (COHP): Energy-resolved visualization of chemical bonding in solids based on density-functional calculations. *J. Phys. Chem.* **1993**, *97*, 8617–8624. [CrossRef]
32. Hermann, F.S. *Pnictogenide and Chalcogenide Zintl Phases via Solid State and Solvothermal Syntheses*; Universitäts-und Landesbibliothek Bonn: Bonn, Germany, 2022.
33. Leon-Escamilla, E.A.; Hurng, W.-M.; Peterson, E.S.; Corbett, J.D. Synthesis, structure, and properties of $Ca_{16}Sb_{11}$, a complex Zintl phase. Twelve other isotypic compounds formed by divalent metals and pnictogens. *Inorg. Chem.* **1997**, *36*, 703–710. [CrossRef]
34. Li, B.; Mudring, A.-V.; Corbett, J.D. Valence compounds versus metals. Synthesis, characterization, and electronic structures of cubic Ae_4Pn_3 phases in the systems Ae = Ca, Sr, Ba, Eu; Pn = As, Sb, Bi. *Inorg. Chem.* **2003**, *42*, 6940–6945. [CrossRef] [PubMed]
35. Jain, A.; Ong, S.P.; Hautier, G.; Chen, W.; Richards, W.D.; Dacek, S.; Cholia, S.; Gunter, D.; Skinner, D.; Ceder, G. Commentary: The Materials Project: A materials genome approach to accelerating materials innovation. *APL Mater.* **2013**, *1*, 011002. [CrossRef]
36. Jain, A.; Hautier, G.; Ong, S.P.; Moore, C.J.; Fischer, C.C.; Persson, K.A.; Ceder, G. Formation enthalpies by mixing GGA and GGA + U calculations. *Phys. Rev. B* **2011**, *84*, 045115. [CrossRef]
37. Ong, S.P.; Wang, L.; Kang, B.; Ceder, G. Li−Fe−P−O_2 phase diagram from first principles calculations. *Chem. Mater.* **2008**, *20*, 1798–1807. [CrossRef]
38. Emmerling, F.; Petri, D.; Röhr, C. Neue Arsenide mit As^--Ketten und-Ringen: $BaAs_2$ und $A^IBa_2As_5$ (A^I = K, Rb). *Z. Anorg. Allg. Chem.* **2004**, *630*, 2490–2501. [CrossRef]
39. Bauhofer, W.; Wittmann, M.; Schnering, H. Structure, electrical and magnetic properties of $CaAs_3$, $SrAs_3$, $BaAs_3$ and $EuAs_3$. *J. Phys. Chem. Solids* **1981**, *42*, 687–695. [CrossRef]
40. Schmettow, W.; von Schnering, H.G. Ba_3As_{14}, The First Compound with the Cluster Anion As. *Angew. Chem. Int. Ed. Engl.* **1977**, *16*, 857. [CrossRef]
41. Saal, J.E.; Kirklin, S.; Aykol, M.; Meredig, B.; Wolverton, C. Materials design and discovery with high-throughput density functional theory: The open quantum materials database (OQMD). *Jom* **2013**, *65*, 1501–1509. [CrossRef]
42. Kirklin, S.; Saal, J.E.; Meredig, B.; Thompson, A.; Doak, J.W.; Aykol, M.; Rühl, S.; Wolverton, C. The Open Quantum Materials Database (OQMD): Assessing the accuracy of DFT formation energies. *npj Comput. Mater.* **2015**, *1*, 15010. [CrossRef]
43. von Schnering, H.-G.; Wittmann, M.; Sommer, D. Zur Chemie und Strukturchemie der Phosphide und Polyphosphide. 35 [1]. *Z. Für Anorg. Und Allg. Chem.* **1984**, *510*, 61–71. [CrossRef]
44. Derrien, G.; Tillard, M.; Manteghetti, A.; Belin, C. Phosphorus Oligomerization in Zintl Phases: Synthesis, Crystal Structure, and Bonding Analysis of Mixed Alkali and Alkaline-Earth Metal Phosphides. *Z. Anorg. Allg. Chem.* **2003**, *629*, 1601–1609. [CrossRef]
45. Deller, K.; Eisenmann, B. Die Kristallstruktur des Sr_3As_4. *Z. Fuer Naturforschung Teil B Anorg. Chem. Org. Chem. Biochem. Biophys. Biol.* **1977**, *32*, 1368–1370.
46. Wang, Y.; Calvert, L.; Gabe, E.; Taylor, J. Structure of europium arsenide Eu_5As_4: A more symmetrical version of the Sm_5Ge_4-type structure. *Acta Crystallogr. Sect. B Struct. Crystallogr. Cryst. Chem.* **1978**, *34*, 1962–1965. [CrossRef]
47. Wang, Y.; Calvert, L.; Smart, M.; Taylor, J.; Gabe, E. The structure of trieuropium tetraarsenide. *Acta Crystallogr. Sect. B Struct. Crystallogr. Cryst. Chem.* **1979**, *35*, 2186–2188. [CrossRef]
48. Derrien, G.; Monconduit, L.; Tillard, M.; Belin, C. Pentabarium tetraantimonide, β-Ba_5Sb_4: A more symmetrical arrangement for the Ba_5Sb_4 compound. *Acta Crystallogr. Sect. C Cryst. Struct. Commun.* **1999**, *55*, 1044–1046. [CrossRef]
49. Brechtel, E.; Cordier, G.; Schäfer, H. Ba_5Sb_4-das erste Erdalkalipnictid mit $GdsSi_4$-Struktur/Ba_5Sb_4-The First Alkaline Earth Pnictide with the Gd_5Si_4 Structure Type. *Z. Für Naturforschung B* **1981**, *36*, 1341–1342. [CrossRef]
50. von Schnering, H.; Wittmann, M.; Sommer, D. Eu_3P_4, Sr_3P_4 Und Ba_3P_4, Polyphosphide Mit P_4^{6-}-Ketten in Einer α-$ThSi_2$-Defektstruktur. *Z. Anorg. Allg. Chem.* **1984**, *510*, 61–71. [CrossRef]
51. Zagorac, D.; Müller, H.; Ruehl, S.; Zagorac, J.; Rehme, S. Recent developments in the Inorganic Crystal Structure Database: Theoretical crystal structure data and related features. *J. Appl. Crystallogr.* **2019**, *52*, 918–925. [CrossRef] [PubMed]
52. Cordero, B.; Gómez, V.; Platero-Prats, A.E.; Revés, M.; Echeverría, J.; Cremades, E.; Barragán, F.; Alvarez, S. Covalent radii revisited. *Dalton Trans.* **2008**, *21*, 2832–2838. [CrossRef] [PubMed]
53. Childs, A.B.; Baranets, S.; Bobev, S. Five new ternary indium-arsenides discovered. Synthesis and structural characterization of the Zintl phases $Sr_3In_2As_4$, $Ba_3In_2As_4$, $Eu_3In_2As_4$, $Sr_5In_2As_6$ and $Eu_5In_2As_6$. *J. Solid State Chem.* **2019**, *278*, 120889. [CrossRef]
54. Deyoung, D. 57Fe Mössbauer study of some M2 (M') B2 borides. *J. Phys. Chem. Solids* **1973**, *34*, 139–140. [CrossRef]
55. Kapfenberger, C.; Albert, B.; Pöttgen, R.; Huppertz, H. Structure refinements of iron borides Fe_2B and FeB. *Z. Kristallogr. Cryst. Mater.* **2006**, *221*, 477–481. [CrossRef]

56. Chan, J.Y.; Olmstead, M.M.; Hope, H.; Kauzlarich, S.M. Synthesis, Structure, and Properties of $Eu_{16}Sb_{11}$ and $Eu_{16}Bi_{11}$. *J. Solid State Chem.* **2000**, *155*, 168–176. [CrossRef]
57. Tappe, F.; Schappacher, F.M.; Langer, T.; Schellenberg, I.; Pöttgen, R. Solid Solutions $RE_{16}Rh_{11-x}Z_x$ (RE = La, Ce, Pr, Nd, Sm; Z = Ga, Zn, Cd, In, Sn, Sb, Pb, Bi)—Centrosymmetric n = 2 Variants of Parthé's Homologous Series $A_{5n+6}B_{3n+5}$. *Z. Naturforsch. B* **2012**, *67*, 594–604. [CrossRef]
58. Martinez-Ripoll, M.; Brauer, G. The crystal structure of Sr_5Sb_3. *Acta Crystallogr. Sect. B Struct. Crystallogr. Cryst. Chem.* **1973**, *29*, 2717–2720. [CrossRef]
59. Shannon, R.D. Revised effective ionic radii and systematic studies of interatomic distances in halides and chalcogenides. *Acta Crystallogr. Sect. A Cryst. Phys. Diffr. Theor. Gen. Crystallogr.* **1976**, *32*, 751–767. [CrossRef]
60. He, H.; Tyson, C.; Saito, M.; Bobev, S. Synthesis and structural characterization of the ternary Zintl phases $AE_3Al_2Pn_4$ and $AE_3Ga_2Pn_4$ (AE = Ca, Sr, Ba, Eu; Pn = P, As). *J. Solid State Chem.* **2012**, *188*, 59–65. [CrossRef]
61. Pauling, L. *The Nature of the Chemical Bond: And the Structure of Molecules and Crystals: Introduction to Modern Structural Chemistry*; Cornell University Press: Ithaca, NY, USA, 1960.